Eur. Phys. J. D **8**, 13–18 (2000)

THE EUROPEAN PHYSICAL JOURNAL D

EDP Sciences

Sub-shell distributions of total electron capture and ionization cross-sections in B^{q+} ($q = 1-4$) + H collisions

M. Das[a], M. Purkait, and C.R. Mandal[b]

Department of Physics, Jadavpur University, Calcutta 700 032, India

Received 23 February 1999 and Received in final form 23 May 1999

Abstract. The Classical Trajectory Monte-Carlo (CTMC) simulation method has been employed to calculate the total electron capture cross-sections with sub-shell distributions and ionization cross-sections in collision of $B^{q+}(q = 1-4)$ with ground state atomic hydrogen in the energy range of 10–200 keV/amu. The computed results have been observed to be in reasonable agreement with other existing theoretical and experimental results over the entire energy region considered.

PACS. 34.70.+e Charge transfer

1 Introduction

Inelastic processes involving multi-charged ions with H atom are of interest in fusion energy research. Very recently boron has been identified as one of the competitive plasma facing materials in fusion reactors [1]. So, reliable data for various inelastic cross-sections for the interaction of different charge states of boron with H atom are needed. Despite progress, the knowledge of cross-section data for such processes is still limited [2–11].

Hansen and Dubois [6] have used the two center atomic state expansion method to compute the total as well as partial charge transfer cross-sections in B^{q+}+H (He) (q = 1, 3, 5) interactions in the energy range of 0.1 to 100 keV/amu. Their investigations are confined to the case of the closed shell/sub-shell projectile ions only. Das *et al.* [7] have calculated the charge transfer cross-sections in collision of B^{q+} ($q = 1-5$) and Be^{q+} ($q = 1-4$) with atomic hydrogen in the energy range of 25 to 200 keV/amu in the framework of Boundary Corrected Continuum Intermediate State (BCCIS) approximation and charge transfer cross-sections to each individual sub-shells has also been given in tabular form in their paper. Olson and Salop [8] have employed CTMC method to calculate the charge transfer and ionization cross-sections in collision of B^{q+}, C^{q+}, N^{q+} and O^{q+} ($q \leq 3$) with atomic hydrogen in the energy range of 30–200 keV/amu. In their calculation, the interaction of the active electron with the complex projectile ion is described by a hydrogenic model with effective charge determined from spectroscopic data. In addition, sub-shell distributions of charge transfer cross-sections are not available from their investigations. However, Olson [9] has later calculated the distributions of total electron capture cross-sections into various principal shells and total ionization cross-sections, in course of his studies on ion-Rydberg atom collisions in the velocity range of 1 au and 10 au in the CTMC method. Salop [10] has applied the CTMC method to calculate the charge transfer cross-sections in collisions of B^{4+}, C^{5+} and O^{7+} with atomic hydrogen. Sub-shell distributions of total charge transfer cross-sections have also been reported in this paper. However, Olson [11] has pointed out that l distributions of electron capture cross-sections for a fixed value of n, reported by Salop [10] are unphysical due to *ad hoc* choice of the weight of statistical distributions. Later a consistent approach has been adopted by Olson [11] to determine n, l distributions of electron capture cross-sections in collisions of fully stripped ions in charge states $q = 1$ to 20 at energies 50 and 100 keV/amu respectively. Under the circumstances, we are motivated to apply the CTMC method to calculate total charge transfer cross-sections with sub-shell distributions and ionization cross-sections in collisions of B^{q+} ($q = 1-4$) with atomic hydrogen in ground state in the energy range of 10–200 keV/amu. Here the significant departure from the CTMC method of Olson and Salop [8] is to account for the interaction of the active electron with the partially stripped projectile ion by a non-Coulombian model potential.

Atomic units are used throughout unless otherwise stated.

2 Theory

Collision diagram is shown in Figure 1. Let a, b, μ_T and μ_P are reduced masses related to co-ordinates $\mathbf{r}_{Te}$, $\mathbf{r}_{Pe}$, $\mathbf{R}_T$ and $\mathbf{R}_P$ respectively.

[a] *Present address*: Panskura Banamali College, Panskura, Midnapur, WB, India.

[b] e-mail: `crm@juphys.ernet.in`

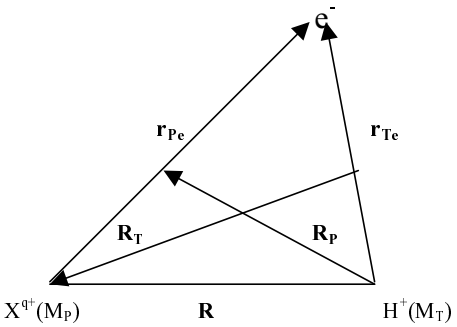

Fig. 1. Co-ordination representation for the reaction B^{q+} $(q = 1{-}4) + H \rightarrow B^{(q-1)+}(nl) + H^+$.

Classical Hamiltonian of the whole system may be written as

$$H = \frac{1}{2a}(p_1^2 + p_2^2 + p_3^2) + \frac{1}{2\mu_T}(p_4^2 + p_5^2 + p_6^2) + V_{Te}(\mathbf{r}_{Te}) + V_{Pe}(\mathbf{r}_{Pe}) + V_{TP}(\mathbf{R}) \quad (1)$$

where,

$$r_{Pe}^2 = (aq_1 - q_4)^2 + (aq_2 - q_5)^2 + (aq_3 - q_6)^2, \quad (2a)$$

$$r_{Te}^2 = q_1^2 + q_2^2 + q_3^2. \quad (2b)$$

Here q_i and p_i $(i = 1{-}3)$ are rectangular co-ordinates and conjugate momenta of the electron relative to the centre of mass of the target system. The corresponding quantities of the projectile ion are q_i and p_i $(i = 4{-}6)$ respectively in the centre of mass of the whole system. Form of the potentials (V_{Te}, V_{TP} and V_{Pe}) are given as

$$V_{Te}(\mathbf{r}_{Te}) = -\frac{1}{r_{Te}} \quad (3a)$$

$$V_{TP}(\mathbf{R}) = \frac{q}{R} \quad (3b)$$

$$V_{Pe}(\mathbf{r}_{Pe}) = -\frac{q}{r_{Pe}} - \frac{e^{-\lambda r_{Pe}}}{r_{Pe}}[(Z - q) + br_{Pe}], \quad (3c)$$

where q is the asymptotic charge and Z is the nuclear charge of the projectile ion. Estimates of the parameters λ and b are described in our earlier investigation [7].

Hamilton's equations of motion may be written as

$$p_i = a\dot{q}_i, \quad i = 1, 2, 3 \quad (4a)$$

$$p_i = \mu_T \dot{q}_i, \quad i = 4, 5, 6. \quad (4b)$$

and

$$\dot{p}_i = \frac{1}{r_{Pe}}\frac{\partial V}{\partial r_{Pe}} a(aq_i - q_{i+3}) - \frac{1}{r_{Te}}\frac{\partial V}{\partial r_{Te}} q_i - \frac{1}{R}\frac{\partial V}{\partial R}\frac{a}{\mu_T}\left(\frac{a}{\mu_T}q_i + q_{i+3}\right), \quad i = 1, 2, 3 \quad (5a)$$

$$\dot{p}_i = \frac{1}{r_{Pe}}\frac{\partial V}{\partial r_{Pe}}(q_i - aq_{i-3}) - \frac{1}{R}\frac{\partial V}{\partial R}\left(q_i + \frac{a}{\mu_T}q_{i-3}\right), \quad i = 4, 5, 6 \quad (5b)$$

where,

$$V = V_{Te}(\mathbf{r}_{Te}) + V_{Pe}(\mathbf{r}_{Pe}) + V_{TP}(\mathbf{R}). \quad (6)$$

These twelve equations in two sets given by equations (4, 5) completely describe the motion of the whole system in centre of mass co-ordinates.

These coupled equations are integrated numerically step by step from $t = -\infty$ to $t = +\infty$. At $t = -\infty$, the target system is unperturbed. So initial values for q_i and p_i $(i = 1{-}6)$ may be assigned in terms of six random numbers [13] from sequence of random numbers. At $t = +\infty$, q_i and p_i $(i = 1{-}3)$ are determined. From these values of q_i and p_i $(i = 1{-}3)$, energies (E_{Te} and E_{Pe}) of the active electron in the sub-systems *i.e.* electron – target ion and electron – projectile ion respectively. Then the final channels are distinguished as described by Olson and Salop [8]. If N_T is the total number of trajectories calculated and N_R is the number of trajectories to satisfy the condition for a particular final channel, the cross-section for the corresponding final channel is given by

$$\sigma_R = \left(\frac{N_R}{N_T}\right)\pi b_{max}^2, \quad (7)$$

where b_{max} is the maximum impact parameter beyond which no reaction takes place.

In the CTMC calculations, sub-shell distributions of total capture cross-sections have been estimated following Becker and Mackellar [12] together with the normalization of the classical angular momentum as prescribed by Olson [11].

3 Results

To check the accuracy of our developed computer CTMC code, we have reproduced the results of Schultz *et al.* [5] within 5% in all cases. In addition, we have reproduced the sub-shell distributions of electron capture cross-sections by Olson [11] within 10% in case of collisions of B^{5+} with atomic hydrogen at 50 keV/amu by setting appropriate values to the model potential parameters in our CTMC code.

Total charge transfer and ionization cross-sections in B^{q+} $(q = 1{-}4)$ + H interaction are given in Tables 1 and 2 respectively. Tables 3–7 contain the n, l distribution for charge transfer cross-sections for collisions of different charge states of boron ion with ground state atomic hydrogen at 10, 20, 50, 75 and 100 keV/amu respectively. Charge transfer and ionization cross-sections for B^{q+} $(q = 1{-}4)$ + H interaction are shown in Figures 2–5 respectively in comparison to the other existing results [6–8].

From Tables 1 and 2, we have observed that the importance of ionization cross-section relative to the charge transfer cross-section has been found to decrease with increasing q over the entire energy range considered.

Table 1. Total capture cross-sections (in 10^{-16} cm^2) at different energies (in keV/amu) for different charge states of boron ion.

Energy	Total cross-sections (in 10^{-16} cm^2)			
(keV/amu)	B^+	B^{2+}	B^{3+}	B^{4+}
10	3.76±0.12	6.80±0.18	13.58±0.21	19.06±0.22
20	2.92±0.09	6.33±0.13	13.39±0.20	18.77±0.22
50	1.13±0.05	3.75±0.11	8.38±0.16	13.53±0.20
75	0.547±0.03	1.52±0.05	4.24±0.12	7.66±0.16
100	0.288±0.02	0.613±0.04	1.89±0.09	3.73±0.11
200	0.043±0.01	0.078±0.01	0.151±0.02	0.322±0.03

Table 2. Total ionization cross-sections (in 10^{-16} cm^2) at different energies (in keV/amu) for different charge states of boron ion.

Energy	Total cross-sections (in 10^{-16} cm^2)			
(keV/amu)	B^+	B^{2+}	B^{3+}	B^{4+}
10	0.54±0.06	0.179±0.06	0.304±0.06	0.233±0.05
20	1.39±0.08	0.545±0.06	0.32±0.06	0.282±0.08
50	3.19±0.11	2.84±0.14	2.56±0.16	2.83±0.18
75	3.12±0.10	4.10±0.16	5.43±0.19	6.17±0.23
100	2.88±0.10	4.04±0.16	6.18±0.24	8.00±0.24
200	2.20±0.09	2.65±0.07	5.07±0.14	7.94±0.24

Table 3. State selective CTMC charge transfer cross-sections (in cm^2) for B^{q+}+H ($q = 1-4$) interaction at 10 keV/amu. $a(b)$ stands for $a \times 10^b$. Σ stands for the sum of the cross-sections of all higher excited states.

		Cross-sections (cm^2)			
n	l	B^+	B^{2+}	B^{3+}	B^{4+}
1	0				
2	0	—	1.05(−16)	2.35(−16)	2.50(−17)
2	1	3.09(−16)	4.52(−16)	5.34(−16)	6.74(−17)
3	0	1.65(−18)	1.30(−17)	7.28(−17)	1.44(−16)
3	1	7.39(−18)	2.77(−17)	1.41(−16)	3.53(−16)
3	2	5.04(−18)	3.37(−17)	2.94(−16)	10.32(−16)
4	0	6.96(−19)	1.65(−18)	9.22(−18)	2.99(−17)
4	1	2.35(−18)	5.19(−18)	1.03(−17)	3.64(−17)
4	2	3.31(−18)	5.59(−18)	1.52(−17)	6.85(−17)
4	3	1.65(−18)	1.65(−18)	1.03(−17)	7.17(−17)
5	0			1.65(−18)	5.48(−18)
5	1			5.39(−18)	8.70(−18)
5	2			3.83(−18)	1.30(−17)
5	3			1.65(−18)	1.03(−17)
5	4			1.04(−18)	8.17(−18)
Σ		4.50(−17)	3.41(−17)	2.15(−17)	3.25(−17)
Total		3.76(−16)	6.80(−16)	13.58(−16)	19.06(−16)

Table 4. Same as for Table 3 except in 20 keV/amu.

		Cross-sections (cm^2)			
n	l	B^+	B^{2+}	B^{3+}	B^{4+}
1	0				
2	0	—	0.54(−16)	1.11(−16)	3.09(−17)
2	1	2.13(−16)	3.96(−16)	4.51(−16)	1.06(−16)
3	0	3.74(−18)	1.57(−17)	4.67(−17)	5.05(−17)
3	1	1.07(−17)	3.84(−17)	1.47(−16)	2.42(−16)
3	2	4.35(−18)	4.91(−17)	4.44(−16)	10.62(−16)
4	0	8.70(−19)	4.69(−18)	1.25(−17)	2.17(−17)
4	1	3.48(−18)	1.03(−17)	2.88(−17)	3.83(−17)
4	2	2.00(−18)	9.74(−18)	2.34(−17)	9.35(−17)
4	3	—	7.39(−18)	2.01(−17)	1.39(−16)
5	0			2.17(−18)	8.70(−18)
5	1			6.00(−18)	9.22(−18)
5	2			7.04(−18)	1.47(−17)
5	3			2.69(−18)	6.00(−18)
5	4			6.52(−18)	1.36(−17)
Σ		5.9(−17)	5.0(−17)	2.98(−17)	4.95(−17)
Total		2.92(−16)	6.33(−16)	13.39(−16)	18.77(−16)

Table 5. Same as for Table 3 except in 50 keV/amu.

		Cross-sections (cm^2)			
n	l	B^+	B^{2+}	B^{3+}	B^{4+}
1	0				2.61(−19)
2	0	—	1.24(−17)	2.87(−17)	2.34(−17)
2	1	6.73(−17)	1.68(−16)	2.15(−16)	1.07(−16)
3	0	1.13(−18)	6.69(−18)	1.39(−17)	1.14(−17)
3	1	7.83(−18)	4.65(−17)	8.09(−17)	8.43(−17)
3	2	2.87(−18)	3.28(−17)	1.94(−16)	3.61(−16)
4	0	4.35(−19)	5.04(−18)	3.91(−18)	7.04(−18)
4	1	3.04(−18)	1.97(−17)	4.35(−17)	4.62(−17)
4	2	8.70(−19)	1.63(−17)	6.52(−17)	1.61(−16)
4	3	—	—	1.04(−17)	1.27(−16)
5	0			5.65(−18)	7.05(−18)
5	1			1.56(−17)	3.04(−17)
5	2			3.74(−17)	6.09(−17)
5	3			5.22(−18)	6.63(−17)
5	4			—	6.00(−18)
Σ		2.95(−17)	6.83(−17)	1.18(−16)	2.53(−16)
Total		1.13(−16)	3.75(−16)	8.38(−16)	13.53(−16)

Table 6. Same as for Table 3 except in 75 keV/amu.

		Cross-sections (cm^2)			
n	l	B^+	B^{2+}	B^{3+}	B^{4+}
1	0				8.70(−20)
2	0	—	1.03(−17)	1.29(−17)	8.18(−18)
2	1	3.48(−17)	5.18(−17)	9.19(−17)	6.22(−17)
3	0	6.09(−19)	3.83(−18)	6.96(−18)	7.05(−18)
3	1	2.61(−18)	1.71(−17)	4.60(−17)	4.49(−17)
3	2	7.83(−19)	1.14(−17)	6.87(−17)	1.57(−16)
4	0		1.31(−18)	4.00(−18)	3.56(−18)
4	1		9.74(−18)	2.56(−17)	2.52(−17)
4	2		7.83(−18)	3.26(−17)	6.78(−17)
4	3		8.70(−20)	6.18(−18)	6.66(−17)
5	0			2.09(−18)	2.26(−18)
5	1			1.57(−17)	1.48(−17)
5	2			1.70(−17)	3.66(−17)
5	3			4.26(−18)	3.96(−17)
5	4			8.70(−20)	4.00(−18)
Σ		1.59(−17)	3.85(−17)	9.00(−17)	2.26(−16)
Total		5.47(−17)	1.52(−16)	4.24(−16)	7.66(−16)

Table 7. Same as for Table 3 except in 100 keV/amu.

		Cross-sections (cm^2)			
n	l	B^+	B^{2+}	B^{3+}	B^{4+}
1	0				5.65(−19)
2	0		7.87(−18)	1.61(−17)	7.92(−18)
				4.80(−18)[a]	
2	1	1.80(−17)	2.05(−17)	5.35(−17)	5.66(−17)
		2.10(−17)[a]		2.93(−17)[a]	
3	0	3.48(−19)	2.52(−18)	6.26(−18)	5.31(−18)
		2.00(−19)[a]		1.90(−18)[a]	
3	1	1.33(−18)		2.66(−17)	
		2.00(−18)[a]	7.39(−18)	8.20(−18)[a]	3.64(−17)
3	2	2.61(−19)	2.09(−18)	1.40(−17)	
		2.00(−19)[a]		1.02(−17)[a]	5.55(−17)
4	0		9.57(−19)	2.87(−18)	2.87(−18)
4	1		3.57(−18)	1.38(−17)	2.19(−17)
4	2		8.70(−19)	7.74(−18)	3.02(−17)
4	3		—	6.09(−19)	1.28(−17)
5	0			1.48(−18)	2.17(−18)
5	1			7.83(−18)	1.36(−17)
5	2			4.17(−18)	1.74(−17)
5	3			4.35(−19)	8.78(−18)
5	4			—	4.35(−19)
Σ		8.90(−18)	1.55(−17)	3.45(−17)	1.01(−16)
Total		2.88(−17)	6.13(−17)	1.89(−16)	3.73(−16)
		2.34(−17)[a]		5.44(−17)[a]	

[a] The results of Hansen and Dubois [6].

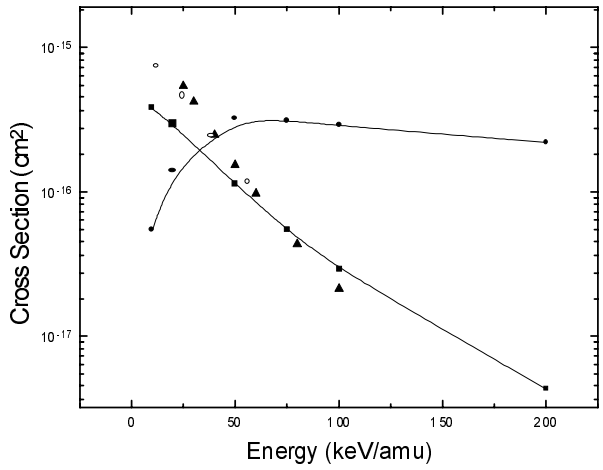

Fig. 2. Variation of capture and ionization cross-sections with energies for B^++H interaction. Theory for capture (■–■–■), CTMC (present); (▲) the results of BCCIS method of Das *et al.* [7]; (○) the results of Hansen and Dubois [6]. Theory for ionization (●– ● –●), CTMC (present).

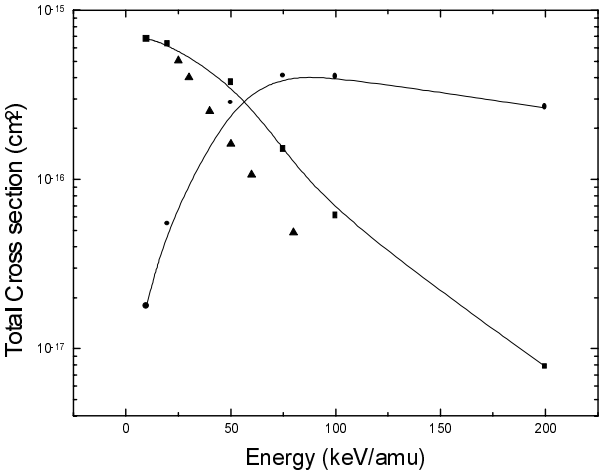

Fig. 3. Variation of capture and ionization cross-sections with energies for B^{2+}+H interaction. Theory for capture (■–■–■), CTMC (present); (▲) the results of BCCIS method of Das *et al.* [7]. Theory for ionization (●– ● –●), CTMC (present).

This is justified because the capture probability enhances as the strength of the potential between the active electron and projectile ion increases. Present CTMC results for electron capture in B^++H interaction are compared with the theoretical results of Hansen and Dubois [6] and of Das *et al.* [7] in Figure 2. Below 100 keV/amu, there is an excellent agreement with all available results. However, discrepancy arises above 100 keV/amu. In Figure 3, the present CTMC results for electron capture in B^{2+}+H interaction are compared only with the results of Das *et al.* [7]. CTMC results are somewhat larger than the above existing results and discrepancy increases with energies. However, the variation of the cross-sections with energies for both calculations have similar trend. Due to non-availability of any other ionization results for $B^{1+,2+}$+H interaction,

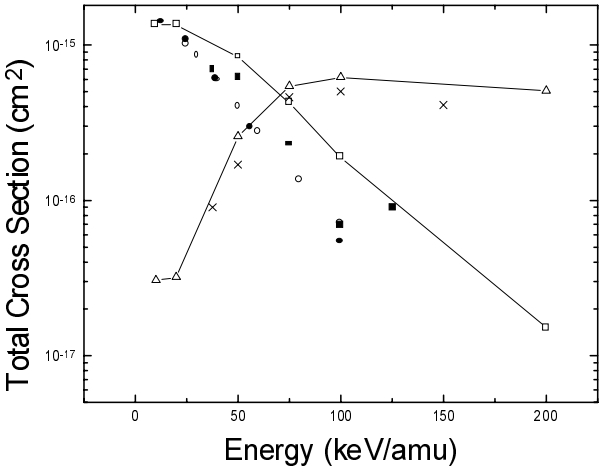

Fig. 4. Variation of capture and ionization cross-sections with energies for B^{3+}+H interaction. Theory for capture (□–□–□), CTMC (present); (○) the results of BCCIS method of Das *et al.* [7]; (●) the results of Hansen and Dubois [6]; (■) prior CTMC results of Olson and Salop [8]. Theory for ionization (△–△–△) CTMC (present); (×) prior CTMC results of Olson and Salop [8].

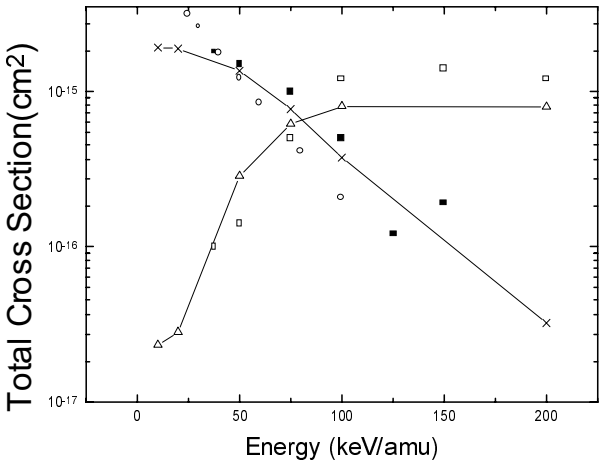

Fig. 5. Variation of capture and ionization cross-sections with energies for B^{4+}+H interaction. Theory for capture (×–×–×), CTMC (present); (○) the results of BCCIS method of Das *et al.* [7]; (■) prior CTMC results of Olson and Salop [8]. Theory for ionization (△–△–△), CTMC (present); (□) prior CTMC results of Olson and Salop [8].

we have displayed our results only in the same Figures 2 and 3 respectively. Results for charge transfer and ionization cross-sections in collision of B^{3+} with atomic hydrogen are drawn in Figure 4. In this case, our present CTMC results for charge transfer have close agreement with the results of Hansen and Dubois [6] and the results of Das *et al.* [7] at lower energies but discrepancy enhances at higher energies. However, marked discrepancies are observed in the variation of cross-sections both for capture and ionization with energies between the present CTMC results and the results of Olson and Salop [8]. From Figure 5, we have observed that both results in CTMC method have closer agreement in the case of B^{4+}+H interaction. However, disagreements of our CTMC results with those of Hansen and Dubois [6] (where available) at higher energies may be due to the difficulties in achieving proper convergence of the used basis set in a coupled state calculation.

In case of closed shell/sub-shell configuration of incoming projectile ion (B^{+}, B^{3+}), the agreement between the classical and quantum results are excellent than in comparison to the open shell structure of the projectile ion (B^{2+}, B^{4+}). This may be due to the fact that the estimate of a model potential for an electron in closed shell structure ion is more accurate than an electron in an ion with open shell structure. From Figures 4 and 5, we observe that the discrepancy between our new CTMC results and the prior results of Olson and Salop [8] both for capture and ionization gradually diminishes as the asymptotic charge of the projectile ion increases to $q = 3$ and 4. This is expected because non-Coulombian model potential is more realistic in comparison to a Coulomb potential in hydrogenic model and the effect of non-Coulombian part of the potential gradually diminishes as the number of passive electrons in the projectile ion decreases.

Almost at all energies, maximum contribution of the cross-section comes from $n = 2$ shell for B^{+} and B^{2+} ions respectively. For B^{3+} impact, $n = 2$ and $n = 3$ shells are quite competitive. However, at lower energies charge transfer into $n = 3$ shell is more favoured. As impact energy increases, $n = 2$ shell overcomes the situation. For B^{4+} interaction, capture into $n = 3$ shell has the dominating effect. All these observations are in conformity with earlier investigations [6,7] and may be explained in terms of resonance or available near resonance of binding energy and velocity matching of the active electron in the initial and final states. In case of l distributions for a fixed value of n, we may find that, for lower values of n, contributions are maximum for larger l values. In contrast, lower values of l take significant share for large values of n. All these characteristic features may be explained in terms of hard and soft collisions [11]. Though the present CTMC results of Olson and Salop [8], sub-shell distributions of total electron capture cross-sections have the same features as prescribed by Olson [11].

4 Concluding remarks

Results obtained by CTMC method for total charge transfer cross-sections have been observed to be quite competitive to quantum mechanical calculations over a certain range of energies. More works may be carried out to find out the validity criteria. However, data for distribution of charge transfer cross-sections into different sub-shells may be a reasonable estimate as may be concluded in comparison to other existing results. Due to non-availability of any other results for ionization for the same processes, it is very difficult to draw any general conclusion for this reaction. So more theoretical and experimental works are needed for studying inelastic collisions of partially stripped ions with neutral atoms.

One of us (CRM) would like to thank the department of Science and Technology (Govt. of India), New Delhi, India for their support of this work through grant No. SP/S2/L03/95. MP also acknowledges to the University Grant Commission, New Delhi, India for providing the research fellowship.

References

1. *Atomic and Molecular Processes in Fusion Edge Plasmas*, edited by R.K. Janev (Plenum Press, New York, 1995).
2. D.R. Schultz *et al.*, Phys. Scripta T **37**, 89 (1991).
3. K. Katsonis, G. Maynard, R.K. Janev, Phys. Scripta T **37**, 80 (1991).
4. W. Fritsch, Phys. Scripta T **62**, 59 (1996).
5. D.R. Schultz, P.S. Krstić, C.O. Reinhold, Phys. Scripta T **62**, 69 (1991).
6. J.P. Hansen, A. Dubois, Phys. Scripta T **62**, 55 (1996).
7. M. Das, M. Purkait, C.R. Mandal, Phys. Rev. A **57**, 3573 (1998).
8. R.E. Olson, A. Salop, Phys. Rev. A **16**, 531 (1977).
9. R.E. Olson, J. Phys. B **13**, 483 (1980).
10. A. Salop, J. Phys. B **12**, 919 (1979).
11. R.E. Olson, Phys. Rev. A **24**, 1726 (1981).
12. R.L. Becker, A.D. Mackellar, J. Phys. B **17**, 3923 (1984) and reference therein.
13. G. Peach, S.L. Willis, M.R.C. McDowell, J. Phys. B **18**, 3921 (1985).